# Electrical activation and spin coherence of ultra low dose antimony implants in silicon

T. Schenkel[1], A. M. Tyryshkin[2], R. de Sousa[3], K. B. Whaley[3], J. Bokor[1, 4], J. A. Liddle[1], A. Persaud[1], J. Shangkuan[1,3], I. Chakarov[5], and S. A. Lyon[2]

[1]E. O. Lawrence Berkeley National Laboratory, Berkeley, CA 94720

[2] Department of Electrical Engineering, Princeton University, Princeton, NJ 08544

[3]Department of Chemistry and Pitzer Center for Theoretical Chemistry, University of California, Berkeley, CA 94720

[4]Department of Electrical Engineering and Computer Science, University of California, Berkeley, Ca 94720

[5]Silvaco International, 4701 Patrick Henry Dr., Santa Clara, CA 95054

We implanted ultra low doses (0.2 to $2\times10^{11}$ $cm^{-2}$) of Sb ions into isotopically enriched $^{28}Si$, and probed electrical activation and electron spin relaxation after rapid thermal annealing. Strong segregation of dopants towards both $Si_3N_4$ and $SiO_2$ interfaces limits electrical activation. Pulsed Electron Spin Resonance shows that spin echo decay is sensitive to the dopant profiles, and the interface quality. A spin decoherence time, $T_2$, of 1.5 ms is found for profiles peaking 25 nm below a $Si/SiO_2$ interface, increasing to 2.1 ms when the surface is passivated with hydrogen. These measurements provide benchmark data for the development of devices in which quantum information is encoded in donor electron spins.

[1] Email: T_Schenkel@LBL.gov

Spins of electrons bound to donor atoms in silicon at low temperature are promising candidates for the development of quantum information processing devices [1-3]. This is due to their long decoherence times, and the potential to leverage fabrication finesse in a silicon transistor paradigm. Recently, relatively long transverse relaxation times ($T_2$) were determined for electron spins in pulsed electron spin resonance (ESR) studies of phosphorous donors in isotopically enriched silicon. Here, donors were present as a random background doping across $^{28}Si$ epi layers and $T_2$ extrapolated to 60 ms for isolated donors [3]. Formation of test devices for quantum information processing requires the integration of individual dopant atoms with a control and readout infrastructure. Donor array fabrication is being addressed by ion implantation [4-6] and scanning probe based hydrogen lithography [7, 8]. Dopant spacing depends on the choice of entangling interactions between quantum bits (qubits) and ranges from 20 to over 100 nm, corresponding to ultra low ion implantation doses of $<10^{10}$ to $2.5\times10^{11}$ $cm^{-2}$. In this letter, we report on electrical activation following rapid thermal annealing (RTA) of ultra low dose $^{121}Sb$ implants and correlate electron spin relaxation times with the dopant distribution below an interface and with the interface quality.

We processed wafers with 10 μm thick, $^{28}Si$ enriched epi layers (500 ppm $^{29}Si$) on p-type natural silicon (100) and natural silicon control wafers (100), both with impurity concentrations $\leq 2\times10^{14}$ $cm^{-3}$. Standard CMOS processes were followed for formation of 5-10 nm thick thermal $SiO_2$, or $Si_3N_4$ layers. Typical densities of trapped charges and interface traps were 1 to $2\times10^{11}$ $cm^{-2}$ for the thermal oxides, and at least an order of magnitude higher for $Si_3N_4$. $^{121}Sb$-ion implantation with $2\times10^{10}$, $10^{11}$ and $2\times10^{11}$ $cm^{-2}$ was conducted with implant energies of 120 keV and 400 keV. A tilt angle of zero

degrees was selected because it will likely be required for single ion placement [4]. $^{121}$Sb was used to avoid any ambiguity of results due to $^{31}$P background in $^{28}$Si epi layers. RTA for repair of implant damage and substitutional incorporation of dopants into the silicon lattice, i. e., electrical activation, was performed with an AGA Heatpulse 610. No effect of the annealing ambient ($N_2$, $N_2/H_2$, or Ar) on carrier profiles was observed. Following annealing, control samples were characterized by Spreading Resistance Analysis (SRA) [9]. Elemental depth profiling with Secondary Ion Mass Spectrometry (SIMS) was impractical due to sensitivity limitations in the analysis of profiles with peak concentrations of $10^{16}$ Sb-atoms/cm$^3$ and below. As-implanted depth profiles were simulated using a dynamic Monte Carlo model [10]. Electron spin relaxation in $^{28}$Si samples was probed by pulsed ESR in an X-band (9.7 GHz) Bruker EPR spectrometer at temperatures of 5 to 10° K. Standard 2-pulse echo and inversion recovery experiments were used to measure $T_1$ and $T_2$ relaxation times, respectively [3]. Results from spin counting by ESR were consistent with SRA results.

Figure 1 a) shows SRA depth profiles of $^{121}$Sb implanted at 120 keV and a dose of $10^{11}$ cm$^{-2}$ after RTA (1000° C, 10 s, $N_2$) together with a simulation of the as-implanted profile. Samples were prepared with layers of $Si_3N_4$ (8 nm) or thermal $SiO_2$ (5 nm). We define the electrical activation ratio as the ratio between the carriers from an integrated, background corrected SRA profile, and the implanted dose. Very low activation ratios of 0.8% and 0.1% are found for the samples annealed in the presence of an $SiO_2$ layer and an $Si_3N_4$ layer, respectively. The profiles show surprisingly strong dopant redistribution towards the dielectric-silicon interfaces. The bulk equilibrium diffusivity for antimony in silicon at 1000° C is relatively low, $10^{-15}$ cm$^2$/s, and would yield only insignificant dopant

movement during RTA [11]. Antimony has been found to diffuse largely through a vacancy mechanism [11]. Therefore, a higher degree of segregation for the vacancy injecting $Si_3N_4$ interface compared to the interstitial injecting $SiO_2$ is expected. The behavior of antimony is complementary to phosphorous, which diffuses mostly through an interstitial mechanism, and where the opposite effect of diffusion retardation by annealing under nitridation conditions was recently reported also for ultra low dose implants [5].

In Figure 1 b) , we show SRA depth profiles from samples implanted with $^{121}Sb$ ($2\times10^{11}$ $cm^{-2}$) at 400 keV and for a series of annealing conditions ranging from 625 C° for 10 s to a spike anneal at 1100° C. Very strong segregation drives the dopant profile towards the interface, but due to the greater as-implanted depth, a significant fraction of dopants does not reach the interface upon annealing and is electrically active. Annealing at 1000° C for 10 s yields the highest activation ratio of 70 %. Competing processes of dopant segregation and incorporation into the silicon lattice can not be resolved without depth profiles of elemental distributions. The activation ratio increases with increasing annealing temperature, in contrast to recent studies of high dose ($4\times10^{14}$ $cm^{-2}$) Sb implants, where anneals at 700-850° C for 10 s achieved >90% activation [12].

Electron spin relaxation times were measured for shallower (average depth of 21 nm after RTA) and deeper (average depth of 64 nm) $^{121}Sb$ implants in $^{28}Si$ with $SiO_2$ interface. Figure 2 shows the six-line ESR spectrum of implanted $^{121}Sb$ donors with splitting arising from hyperfine interaction with the nuclear spin (I=5/2) of $^{121}Sb$. Most of the relaxation measurements were done at the M=1/2 hyperfine line but the relaxation times were identical on other lines. For shallower donors (120 keV at $2\times10^{10}$ $cm^{-2}$ dose

and annealed at 1000° C for 10 s and 60 s in $N_2$), the spin relaxation times $T_1 = 15 \pm 2$ ms and $T_2 = 0.3 \pm 0.03$ ms were found at 5.2° K. For deeper implants (400 keV at $2\times10^{11}$ $cm^{-2}$ dose and annealed at 1000° C for 10 s) a much longer $T_2 = 1.5 \pm 0.1$ ms was measured while $T_1 = 16 \pm 1$ ms did not change.

The oxide layer of $^{28}Si$ samples was then removed by etching in a hydrofluoric acid solution, resulting in a hydrogen terminated silicon (100) surface of modest quality (compared to Si-111) [13, 14]. The electrical properties of the H-Si interface were not probed here, but typical interface trap densities below $10^9$ $cm^{-2}$ have previously been reported [15]. Following hydrogen passivation, $T_2$ increased to 2.1 ms for the 400 keV implants, and to 0.75 ms for the 120 keV implants. We summarize our results in Table 1.

Dopants diffuse through interaction with interstitials and vacancies. In the ultra low dose, intrinsic implant regime, dopant redistribution during RTA is affected by defect injection from the dielectric-silicon interface, and by the interaction of dopants with point defects that did not recombine following the slow down of implanted ions (i. e., transient enhanced diffusion, TED) [11, 16]. For low dose phosphorous implants and annealing in the presence of an $Si_3N_4$/Si interface, diffusion retardation through injection of vacancies dominates over TED [5]. For antimony, point defect formation is enhanced in collision cascades with the heavier Sb ions. Recombination of vacancies and interstitials is incomplete for ultra low dose implants [16]. We find that dopant redistribution is dominated by TED, and diffusion retardation due to injection of interstitials from the $Si/SiO_2$ interface is insignificant. Dopants are driven towards the interface where they are not electrically active [17]. From the SRA profiles in Figure 1, we estimate an effective diffusion coefficient of $10^{-11}$ $cm^2/s$, $10^4$ higher than the equilibrium value for Sb in silicon

at 1000° C. Quantum computer test structures require both efficient electrical activation of dopants and retention of initial dopant positions during thermal processing. The results shown here fulfill neither requirement, but enable testing of single spin readout architectures with reasonable device yields. Further optimization of thermal processing with defect engineering and control of interface properties is needed to improve activation and suppress dopant redistribution.

Donor electron spin relaxation is correlated both with the average distance of dopants from an interface and with the interface quality (Table 1). The fact that removal of the oxide layer and H-passivation of the interface lead to a significant increase in $T_2$ allows us to conclude that it is coupling to paramagnetic defects in the oxide and at $Si/SiO_2$ interfaces which limits $T_2$ for both shallow and deeper dopant distributions. A likely mechanism is fluctuating magnetic fields due to spin flips of paramagnetic defects and the loading and unloading of traps at the interface and in the oxide [18]. At much reduced interface trap levels for the H-Si surface, coherence is likely limited by instantaneous diffusion, i.e. magnetic dipole coupling of neighboring dopant atoms [2, 3], and possibly other effects that have not been quantified. We estimate the effect of nuclear spins of hydrogen atoms at a coverage of $6.8\times10^{14}$ $cm^{-2}$ for an H-Si (100) surface on donor electron spin coherence with a spectral diffusion model [2]. This process is expected to limit $T_2$ to about 20 ms for the profile shown in Figure 1 a), and to 1 s for the profile peaking at a depth of 25 nm below an H-Si interface (Figure 1 b) and is probably not important in the present case.

In summary, transient enhanced diffusion during annealing of ultra low dose antimony implants leads to strong dopant segregation to both $SiO_2$ and $Si_3N_4$ interfaces,

limiting electrical activation at low implant energies. Activation ratios of 70% are achieved for 400 keV implants. The transverse electron spin relaxation time, $T_2$, increases when dopants are placed deeper below a thermal $SiO_2$ interface, and hydrogen passivation of the silicon surface yields an even longer $T_2$ of 2.1 ms, indicating that spin flips in paramagnetic defects limit coherence in the presence of a $Si/SiO_2$ interface. Spin coherence times well in excess of 1 ms are readily achieved with standard CMOS processing, enabling tests of quantum information processing architectures with donor electron spin qubits.

**Acknowledgments**

We thank T. C. Shen for stimulating discussions, and the staff of the UC Berkeley Microlab for their technical support. This work was supported by NSA under ARO contract number MOD707501, the U. S. DOE under contract No. DE-AC02-05CH11231, and NSF.

**References**

[1] B. E. Kane, Nature 393, 133 (1998); R. Vrijen, E. Yablonovitch, K. Wang, H. W. Jiang, A. Balandin, V. Roychowdhury, T. Mor, and D. DiVincenzo, Phys. Rev. A, 62, 12306 (2000)

[2] S. Das Sarma, R. de Sousa, X. Hu, and B. Koiller, Solid State Comm. 133, 737 (2005)

[3] A. M. Tyryshkin, S. A. Lyon, A. V. Astashkin, and A. M. Raitsimring, Phys. Rev. B 68, 193207 (2003)

[4] A. Persaud, S. J. Park, J. A. Liddle, J. Bokor, I. W. Rangelow, and T. Schenkel,

Nano Letters 5, 1087 (2005)

[5] A. Persaud, S. J. Park, J. A. Liddle, I. W. Rangelow, J. Bokor, R. Keller, F. I. Allen, D. H. Schneider, and T. Schenkel, Quantum Info. Process. 3, 233 (2004)

[6] D. N. Jamieson, C. Yang, T. Hopf, S. M. Hearne, C. I. Pakes, S. Prawer, M. Mitic, E. Gauja, S. E. Andersen, F. E. Hudson, A. S. Dzurak, and R. G. Clark, Appl. Phys. Lett. 86, 202101 (2005)

[7] T. C. Shen, J. S. Kline, T. Schenkel, S. J. Robinson, J.-Y. Ji, C. Yang, R.-R. Du, J. R. Tucker, J. Vac. Sci. Technol. B 22, 3182, (2004)

[8] F. J. Ruess, L. Overbeck, M. Y. Simmons, K. E. J. Goh, A. R. Hamilton, T. Hallam, S. R. Schofield, N. J. Curson, and R. G. Clark, Nano Letters 4, 1969 (2004)

[9] Solecon Laboratories, Reno, NV

[10] I.R. Chakarov and R.P. Webb, Rad. Eff. Def. Solids 130, 447 (1994)

[11] N. Cowern, and C. Rafferty, MRS Bulletin Vol. 25, No. 6, 39 (2000); A. Ural, P. B. Griffin, J. D. Plummer, J. Appl. Phys. 85, 6440 (1999)

[12] T. Alzanki, R. Gwilliam, N. Emerson, Z. Tabatabaian, C. Jeynes, and B. J. Sealy, Semicond. Sci. Technol. 19, 728 (2004)

[13] J. C. Kim, J.-Y. Ji, J. S. Kline, J. R. Tucker, and T.-C. Shen, Appl. Surf. Sci. 220, 293 (2003)

[14] K. Eng, R. N. McFarland, and B. E. Kane, pre-print archive, cond-mat/0501608

[15] E. Yablonovitch, D. L. Allara, C. C. Chang, T. Gmitter, and T. B. Bright, Phys. Rev. Lett. 57, 249 (1986)

[16] L. Pelaz, G. H. Gilmer, V. C. Venezia, H. J. Gossman, M. Jaraiz, and J. Barbolla, Appl. Phys. Lett. 74, 2017 (1999)

[17] J. Dabrowski, H.-J. Müssig, V. Zavodinsky, R. Baierle, and M. J. Caldas, Phys. Rev. B 65, 245305 (2002)

[18] S. T. Chang, J. K. Wu, and S. A. Lyon, Appl. Phys. Lett. 48, 662, (1986); A. Stesmans and V. V. Afanas'ev, Phys. Rev. B 57, 10030 (1998)

**Figure and table captions:**

Figure 1: SRA depth profiles of carrier concentrations for a) $10^{11}$ $cm^{-2}$, 120 keV $^{121}Sb$ implants with thin films of $SiO_2$, and $Si_3N_4$ after RTA (1000° C, 10 s, $N_2$), together with a Monte Carlo simulation of the as-implanted profile. b) SRA profiles (linear scale) for $2\times10^{11}$ $cm^{-2}$, $^{121}Sb$ implants (400 keV) and a series of annealing conditions.

Figure 2.: The 2-pulse electron spin echo (ESE) decay for $^{121}Sb$ donors in $^{28}Si$ (400 keV, dose $2\times10^{11}$ $cm^{-2}$, annealed at 1000° C for 10 s) measured at the M = +1/2 line in the ESR spectrum at 5.2° K. Because the ESE signal decay is strongly suppressed at long $\tau > 0.5$ ms by magnetic field noise [3], the exponential fit (dashed line) was calculated using only $\tau < 0.5$ ms and resulted in $T_2 = 2.1$ ms. The insert shows an ESR spectrum of $^{121}Sb$, consisting of six narrow (<0.2 G) lines split by hyperfine interaction with the nuclear spin (I=5/2) of $^{121}Sb$. The broad feature in the centre of the spectrum is from surface defects due to sample preparation.

Table 1: Summary of activation ratios and decoherence times for nitride, oxide and hydrogen passivation of $^{28}Si$ surfaces (100).

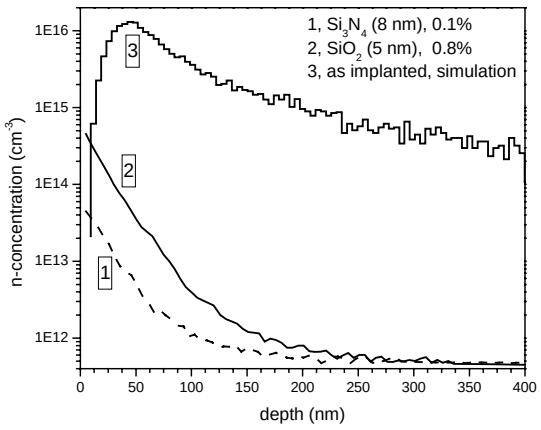
1, Si3N4 (8 nm), 0.1%
2, SiO2 (5 nm), 0.8%
3, as implanted, simulation
n-concentration (cm-3)
depth (nm)
1E16
1E15
1E14
1E13
1E12
0
50
100
150
200
250
300
350
400
1
2
3

Figure 1 a)

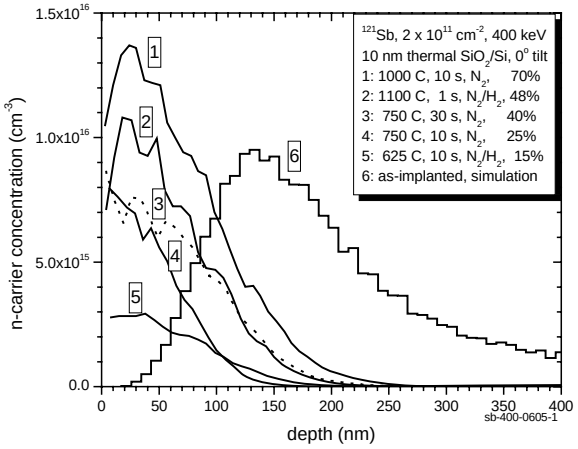
1.5x10^16
1.0x10^16
5.0x10^15
0.0
n-carrier concentration (cm^-3)
0
50
100
150
200
250
300
350
400
depth (nm)
sb-400-0605-1
121Sb, 2 x 10^11 cm^-2, 400 keV
10 nm thermal SiO2/Si, 0° tilt
1: 1000 C, 10 s, N2, 70%
2: 1100 C, 1 s, N2/H2, 48%
3: 750 C, 30 s, N2, 40%
4: 750 C, 10 s, N2, 25%
5: 625 C, 10 s, N2/H2, 15%
6: as-implanted, simulation
1
2
3
4
5
6

Figure 1 b)

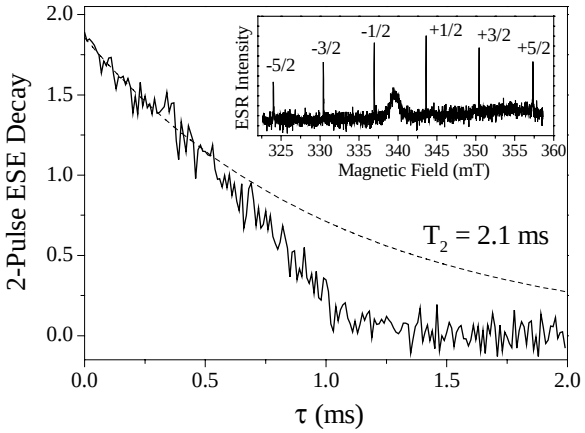
2-Pulse ESE Decay
τ (ms)
T2 = 2.1 ms
ESR Intensity
Magnetic Field (mT)
-5/2
-3/2
-1/2
+1/2
+3/2
+5/2

Figure 2.

| Interface | Average dopant depth (nm) | Activation ratio | $T_1$ (ms) at 5.2° K | $T_2$ (ms) at 5.2° K |
|---|---|---|---|---|
| $Si_3N_4$ | 21 | 0.1 % | - | - |
| $SiO_2$ | 21 | 0.8 % | 15 ± 2 | 0.30 ± 0.03 |
| H-Si | 21 | - | 16 ± 2 | 0.75 ± 0.04 |
| $SiO_2$ | 64 | 70 % | 16 ± 1 | 1.5 ± 0.1 |
| H-Si | 64 | - | 14 ± 1 | 2.1 ± 0.1 |

Table 1